J|A|C|S ARTICLES

Published on Web 10/06/2009

Impacts of the Location and Number of $[Cu(bpy)_2]^{2+}$ Cross-Links on the Emission Photodynamics of $[Ru(bpy)_3]^{2+}$ with Pendant Oligo(aminoethylglycine) Chains

Carl P. Myers,[†] James R. Miller,[‡] and Mary Elizabeth Williams*[,†]

Department of Chemistry, 104 Chemistry Building, and Huck Institutes of the Life Sciences Mass Spectrometry Facility, 3 Althouse Laboratory, The Pennsylvania State University, University Park, Pennsylvania 16802

Received July 3, 2009; E-mail: mbw@chem.psu.edu

Abstract: Multifunctional aminoethylglycine (aeg) derivatized $[Ru(bpy)_3]^{2+}$ complexes with pendant bipyridine (bpy) ligands coordinate Cu^{2+} to form coordinative chain cross-links in a "hairpin loop" motif. In this paper, we report the synthesis and characterization of a series of Ru aeg hairpins in which the relative aeg chain length and number of pendant bpy ligands is varied. Reaction of each of these with Cu^{2+} is monitored using spectrophotometric emission titrations to determine the binding stoichiometry. Coordination of Cu^{2+} causes quenching of the emissive excited state Ru species; the degree of quenching efficiency depends on the location and number of coordinated Cu ions. The heterometallic structures are fully characterized, and using the quantum yields and time-resolved emission following excitation of the Ru complexes in deoxygenated solutions, the radiative (k_r) and nonradiative (k_{nr}) relaxation rates are compared. These data reveal only a shallow decrease in k_{nr} with increasing distance between the Ru and Cu complexes. Activation energies, determined from temperature dependent studies of the time-resolved emission, also increase as the Ru−Cu separation increases, resulting in the smaller nonradiative rates. Together, these data are suggestive of excited state electron transfer as the quenching mechanism and demonstrate that metal coordination self-assembles structures made from modular artificial amino acids can provide controlled arrangements of chromophores, electron donors, and electron acceptors to shuttle electrons in a new approach for mimicking photosynthesis.

Introduction

Nature uses self-assembly of macromolecules built from modular repeating units to organize intricate structures capable of complex functions. For example, photosynthetic organisms have mastered molecular recognition and self-assembly, forming large structures that use light to funnel energy and electrons. Synthetic biomimetic molecules for artificial photosynthesis must be designed to specifically control the relative placement of chromophores and electron donors and acceptors to create long-lived charge-separated states capable of performing chemical work. Multifunctional molecular systems, largely containing covalently linked moieties, have been synthesized to investigate and control photoinduced charge transport;[1−3] large architectures, both inorganic[4−9] and organic,[10−13] have been used to demonstrate the ability to mimic photosynthetic light harvesting.

* To whom correspondence should be addressed. E-mail: .
† Department of Chemistry.
‡ Huck Institutes of the Life Sciences Mass Spectrometry Facility.

(1) (a) Wasielewski, M. R. *J. Org. Chem.* **2006**, *71*, 5051–5066. (b) Wasielewski, M. R. *Chem. Rev.* **1992**, *92*, 435–461. (c) Lewis, F. D.; Letsinger, R. L.; Wasieleski, M. R. *Acc. Chem. Soc.* **2001**, *34*, 159–170.

(2) (a) Meyer, T. J. *Acc. Chem. Res.* **1989**, *22*, 163–170. (b) Alstrum-Acevedo, J. H.; Brennaman, M. K.; Meyer, T. J. *Inorg. Chem.* **2005**, *44*, 6802–6827. (c) Huynh, M. H. V.; Meyer, T. J. *Chem. Rev.* **2007**, *107*, 5004–5064.

(3) (a) Lomoth, R.; Magnuson, A.; Sjodin, M.; Huang, P.; Styring, S.; Hammarstrom, L. *Photosynth. Res.* **2006**, *87*, 25–40. (b) Martin, N.; Sanchez, L.; Illescas, B.; Perez, I. *Chem. Rev.* **1998**, *98*, 2527–2547.

(4) Kodis, G.; Herrerro, C.; Palacios, R.; Marino-Ochoa, E.; Gould, S.; de la Garza, L.; van Grondelle, R.; Gust, D.; Moore, T. A.; Moore, A. L.; Kennis, J. T. M. *J. Phys. Chem. B* **2004**, *108*, 414–425.

(5) (a) Abrahamsson, M. L. A.; Baudin, H. B.; Tran, A.; Philouze, C.; Berg, K. E.; Raymond-Johansson, M. K.; Sun, L.; Akermark, B.; Styring, S.; Hammarstrom, L. *Inorg. Chem.* **2002**, *41*, 1534–1544. (b) Haung, P.; Hogblom, J; Anderlund, M. F.; Sun, L.; Manguson, A.; Styring, S. *J. Inorg. Biochem.* **2004**, *98*, 733–745. (c) Falkenstrom, M; Johansson, O.; Hammarstrom, L. *Inorg. Chim. Acta* **2007**, *360*, 741–750.

(6) (a) Du, P.; Schneider, J.; Jarosz, P.; Zhang, J.; Brennessel, W. W.; Eisenberg, R. *J. Phys. Chem. B* **2007**, *111*, 6887–6894. (b) Lazarides, T.; McCormick, T.; Du, P.; Luo, G.; Lindley, B.; Eisenberg, R. *J. Am. Chem. Soc.* **2009**, *131*, 9192–9194. (c) Du, P.; Schneider, J.; Luo, G.; Brennessel, W. W.; Eisenberg, R. *Inorg. Chem.* **2009**, *48*, 4952–4962. (d) Jarosz, P; Lotito, K.; Schneider, J.; Kumaresan, D.; Schmehl, R.; Eisenberg, R. *Inorg. Chem.* **2009**, *48*, 2420–2428.

(7) (a) Balazs, G. C.; del Guerzo, A.; Schmehl, R. H. *Photochem. Photobiol. Sci.* **2005**, *4*, 89–94. (b) Mellace, M. G.; Fagalde, F.; Katz, N. E.; Hester, H. R.; Schmehl, R. *J. Photochem. Photobiol A: Chem.* **2006**, *181*, 28–32. (c) Wang, X.; Guerzo, A. D.; Baitalik, S.; Simon, G.; Shaw, G. B.; Chen, L. X.; Schmehl, R. *Photosynth. Research* **2006**, *87*, 83–103.

(8) Tran, E.; Cohen, A. E.; Murray, R. W.; Rampi, M. A.; Whitesides, G. M. *J. Am. Chem. Soc.* **2009**, *131*, 2141–2150.

(9) (a) Concepcion, J. J.; Jurss, J. W.; Templeton, J. L.; Meyer, T. J. *Proc. Natl. Acc. Sci. U.S.A.* **2008**, *105*, 17632–17635. (b) Concepcion, J. J.; Brennaman, M. K.; Deyton, J. R.; Lebedeva, N. V.; Forbes, M. D. E.; Papanikolas, J. M.; Meyer, T. J. *J. Am. Chem. Soc.* **2007**, *129*, 6968–6969. (c) Fleming, C. N.; Brennaman, M. K.; Papanikolas, J. M.; Meyer, T. J. *Dalton Trans.* **2009**, *20*, 3903–3910.

By virtue of their size and complexity, these supramolecular structures can be synthetically challenging to make. There have been several recent examples of using relatively weak intermolecular forces (versus covalent bonds) to self-assemble mesoscale structures from molecular and supramolecular components.[14]

Amino acid building blocks are the modular repeat units of biology. Employing biomimetic strategies to drive the formation of large, functional molecules could lead to artificial analogs of natural and technologically important systems. Our aim has been to use artificial analogs of amino acids to exploit straightforward amide coupling chemistries and construct oligopeptides in readily reconfigurable sequences. Ligand-substituted aminoethylglycine is used to build oligomers that, by analogy to molecular recognition and assembly in nature, coordinate transition metal ions and self-assemble into multifunctional supramolecular structures. These are a tractable approach for making highly complex architectures needed to realize artificial photosynthesis.

Assembly of complex supramolecular structures by inorganic coordination chemistry is a promising route for construction of artificial photosynthetic systems because the coordination number and geometry, photochemistry, metal ion lability, redox states, etc. are all tunable based on the ligand and transition metal.[15−18] We have demonstrated that artificial oligopeptides based on the modular ligand-substituted aminoethylglycine (aeg)

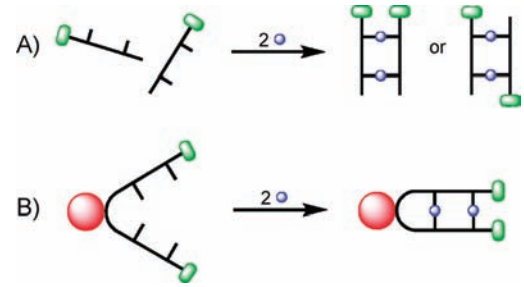

Figure 1. Two motifs for self-assembly of oligopeptides with pendant ligands by metal ion coordination: (A) self-complementary bpy-substituted aeg dipeptides form parallel and antiparallel isomers when cross-linked with Cu^{2+} (blue spheres).[19a] (B) Attachment of aeg strands to $[Ru(bpy)_3]^{2+}$ (red sphere) predirects alignment, Cu^{2+} binds to close the "hairpin loop".

self-assemble into multimetallic structures when transition metal ions coordinate to the pendant ligands.[19,20] Polyfunctional oligopeptides have been used to induce self-assembly of heterometallic structures,[19c,20] or to cause coordinative cross-linking between oligopeptide strands to form double-stranded duplexes linked by multiple metal ions.[19a,c,20] Metal-based recognition and assembly of artificial aeg strands to form duplex structures is shown in Figure 1A: molecular recognition is driven by complementary denticity of the ligands with respect to coordinative saturation of the target metal ion.[19,20] This strategy can result in the formation of parallel and antiparallel isomers. To improve our control over the structural geometries in the metal-linked oligopeptide duplexes, we have begun to design aeg oligopeptides that reduce or eliminate misalignment and isomer formation and that enable facile preparation of heterometallic, multifunctional assemblies. One of our recent approaches[20] has been to take inspiration from hairpin loops in self-complementary nucleic acid sequences.[21] By analogy, we have designed artificial peptide analogs with two complementary ligand substituted aeg chains that coordinatively cross-link the hairpin loop, as in Figure 1B.

In the first study of the "hairpin" motif for construction of heterometallic complexes,[20a] the preparation of $[Ru(bpy)_3]^{2+}$ compounds derivatized with two bipyridine (bpy)-containing aeg substituents was reported. Both aeg strands with a single pendant bpy are substituted from the same ligand in the Ru complex, so that they are preprogrammed for "loop" formation (Figure 1B). Addition of Cu^{2+} or Zn^{2+} ions was shown to coordinatively cross-link the chains, forming heterometallic structures. Time-resolved emission spectroscopy of these revealed that coordination of Cu^{2+} dramatically reduced the $[Ru(bpy)_3]^{2+}$ quantum

(10) (a) Lewis, F. D.; Liu, X.; Wu, Y.; Zuo, X. *J. Am. Chem. Soc.* **2003**, *125*, 12729–12731. (b) Lewis, F. D.; Wu, Y.; Zhang, L.; Zuo, X.; Hayes, R. T.; Wasielewski, M. R. *J. Am. Chem. Soc.* **2004**, *126*, 8206–8215. (c) Zeidan, T. A.; Carmieli, R.; Kelley, R. F.; Wilson, T. M; Lewis, F. D.; Wasielewski, M. R. *J. Am. Chem. Soc.* **2008**, *130*, 13945–13955. (d) Daublain, P.; Siegmund, K.; Hariharan, M.; Vura-Weis, J.; Wasielewski, M. R.; Lewis, F. D.; Shafirovich, V.; Wang, Q.; Raytchev, M.; Fiebig, T. *Photochem. Photobiol. Sci.* **2008**, *7*, 1501–1508.

(11) (a) Funston, A. M.; Silverman, E. E.; Miller, J. R.; Schanze, K. S. *J. Phys. Chem. B* **2004**, *108*, 1544–1555. (b) Paulson, B. P.; Miller, J. R.; Gan, W. X.; Closs, G. *J. Am. Chem. Soc.* **2005**, *127*, 4860–4868. (c) Asaoka, S.; Takeda, N.; Iyoda, T.; Cook, A. R.; Miller, J. R. *J. Am. Chem. Soc.* **2008**, *130*, 11912–11920.

(12) (a) Visoly-Fisher, I.; Daie, K.; Teraznon, Y.; Herrero, C.; Fungo, R.; Otero, L.; Durantini, D.; Silber, J. J.; Sereno, L.; Gust, D.; Moore, T. A.; Moore, A. L.; Lindsay, S. M. *Proc. Natl. Acad. Sci. U.S.A.* **2006**, *103*, 8686–8690. (b) He, J.; Fu, Q.; Lindsay, S.; Ciszek, J. W.; Tour, J. M. *J. Am. Chem. Soc.* **2006**, *128*, 14828–14835. (c) He, J.; Chen, F.; Lindsay, S. *Appl. Phys. Lett.* **2007**, *90*, 072112-1–072112-3. (d) He, J.; Lin, L.; Liu, H.; Zhang, P.; Lee, M.; Sankey, O. F.; Lindsay, S. M. *Nanotechnology* **2009**, *20*, 075102-1–075201-8.

(13) He, J.; Forzani, E. S.; Nagahara, L. A.; Tao, N.; Lindsay, S. *J. Phys.: Condens. Matter* **2008**, *20*, 374120.

(14) (a) Rybtchinski, B.; Sinks, L. E.; Wasielewski, M. R. *J. Am. Chem. Soc.* **2004**, *126*, 12268–12269. (b) Palacios, R. E.; Kodis, G.; Herrero, C.; Ochoa, E. M.; Gervaldo, M.; Gould, S. L.; Kennis, J. T. M.; Gust, D.; Moore, T. A.; Moore, A. L. *J. Phys. Chem. B* **2006**, *110*, 25411–25420. (c) Imahori, H. *J. Phys. Chem. B* **2004**, *108*, 6130–6143.

(15) (a) Jensen, R. A.; Kelley, R. F.; Lee, S. J.; Wasielewski, M. R.; Hupp, J. T.; Tiede, D. M. *Chem. Commun.* **2008**, *16*, 1886–1888. (b) Slone, R. V.; Hupp, J. T.; Stern, C. L.; Albrecht-Schmitt, T. E. *Inorg. Chem.* **1996**, *35*, 4096–4097.

(16) (a) Kryschenko, Y. K.; Seidel, S. R.; Arif, A. M.; Stang, P. J. *J. Am. Chem. Soc.* **2003**, *125*, 5193–5198. (b) Northrop, B. H.; Yang, H. B.; Stang, P. J. *Inorg. Chem.* **2008**, *47*, 11257–11268. (c) Yang, H.; Northrop, B. H.; Zheng, Y.; Ghosh, K.; Lyndon, M. M.; Muddiman, D. C.; Stang, P. J. *J. Org. Chem.* **2009**, *74*, 3524–3527. (d) Ghosh, K.; Hu, J.; White, H. S.; Stang, P. J. *J. Am. Chem. Soc.* **2009**, *131*, 6695–6697.

(17) (a) Kuciauskas, D.; Monat, J. E.; Villahermosa, R.; Gray, H. B.; Lewis, N. S.; McCusker, J. K. *J. Phys. Chem. B* **2002**, *106*, 9347–9358. (b) Khalil, M.; Marcus, M. A.; Smeigh, A. L.; McCusker, J. K.; Chong, H. H. W.; Schoenlein, R. W. *J. Phys. Chem. A* **2006**, *110*, 38–44. (c) Guo, D.; McCusker, J. K. *Inorg. Chem.* **2007**, *46*, 3257–3274. (d) Soler, M.; McCusker, J. K. *J. Am. Chem. Soc.* **2008**, *130*, 4708–4724.

(18) (a) McGarrah, J. E.; Hupp, J. T.; Smirnov, S. N. *J. Phys. Chem. A* **2009**, *113*, 6430–6436. (b) Kelley, R. F.; Lee, S. J.; Wilson, T. M.; Nakamura, Y.; Tiede, D. M.; Osuka, A.; Hupp, J. T.; Wasielewski, M. R. *J. Am. Chem. Soc.* **2008**, *130*, 4277–4284.

(19) (a) Gilmartin, B. P.; Ohr, K.; McLaughlin, R. L.; Koerner, R.; Williams, M. E. *J. Am. Chem. Soc.* **2005**, *127*, 9546–9555. (b) Ohr, K.; Gilmartin, B. P.; Williams, M. E. *Inorg. Chem.* **2005**, *44*, 7876–7885. (c) Gilmartin, B. P.; McLaughlin, R. L.; Williams, M. E. *Chem. Mater.* **2005**, *17*, 5446–5454. (d) Levine, L. A.; Morgan, C. M.; Ohr, K.; Williams, M. E. *J. Am. Chem. Soc.* **2005**, *127*, 16764–16765. (e) Ohr, K.; McLaughlin, R. L.; Williams, M. E. *Inorg. Chem.* **2007**, *46*, 965–974. (f) Levine, L. A.; Youm, H. W.; Yennawar, H. P.; Williams, M. E. *Eur. J. Inorg. Chem.* **2008**, *26*, 4083–4091.

(20) (a) Myers, C. P.; Gilmartin, B. P.; Williams, M. E. *Inorg. Chem.* **2008**, *47*, 6738–6747. (b) Levine, L. A,; Kirin, S. I.; Myers, C. P.; Showalter, S. A.; Williams, M. E. *Eur. J. Inorg. Chem.* **2009**, *5*, 613–621.

(21) (a) Borer, P. N.; Uhlenbeck, O. C.; Dengler, B.; Tinaco, I. *J. Mol. Biol.* **1973**, *73*, 483–496. (b) Hilbers, C. W.; Haasnoot, C. A. G.; de Bruin, S. H.; Joordens, J. J. M.; Van der Marel, G. A.; Van Boom, J. H. *Biochimie* **1985**, *67*, 685–695.

Scheme 1. Oligopeptide Hairpin Substituted Ru Complexes

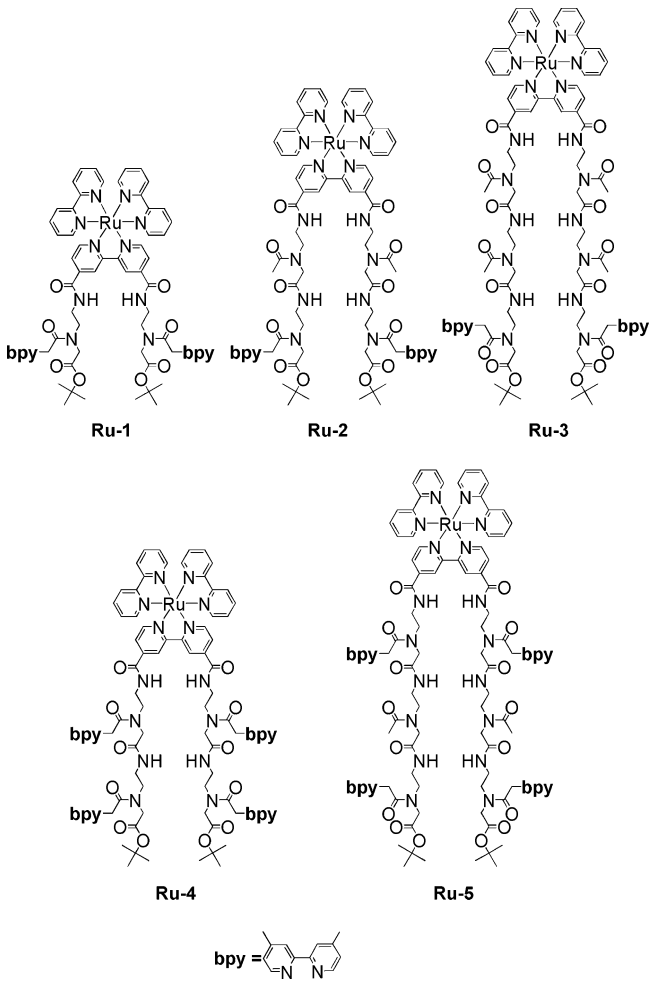

yield and excited state lifetime. Several possible mechanisms could give rise to the excited state quenching of the Ru core. In this paper we leverage the modular, expandable artificial peptide backbone to synthesize a series of molecules and study the photodynamics of these structures, with the ultimate goal of using this understanding to build more complex and potentially useful architectures with long-lived charge separated states capable of performing chemical work.

Our aims here are two-fold. First, since both energy and electron transfer quenching mechanisms are distinctly distant-dependent,[22] solution phase peptide coupling chemistry is used to increase the length of the oligopeptide and therefore the distance between [Ru(bpy)$_3$]$^{2+}$ and [Cu(bpy)$_2$]$^{2+}$. Second, modification of the peptide to contain additional pendant bipyridine ligands and form heterotrimetallic complexes tests the impact on additional redox sites on the photophysical behavior. Scheme 1 shows the series of aeg-modified [Ru(bpy)$_3$]$^{2+}$ hairpin structures that are synthesized and studied in this paper. Time-resolved and temperature-dependent emission spectroscopy are used to understand the role of the structural variation on the emission lifetimes of these complexes. These compounds provide a unique way to vary structure using variable combinations of aeg modular units, and to therefore build increasingly complex heterofunctional architectures. We find that the dynamics point toward photoinduced electron transfer as the dominant quenching mechanism, laying the groundwork for the use of this approach to build large, oligopeptide-linked architectures for artificial photosynthesis.

Experimental Section

Chemicals and Reagents. N-Hydroxybenzotriazole (HOBT) and 1-ethyl-3-(3-dimethylaminopropyl)carbodiimide hydrochloride (EDC) were purchased from Advanced ChemTech. O-Benzotriazole-N,N,N',N'-tetramethyl-uronium-hexafluorophosphate (HBTU) was purchased from NovaBiochem. Copper(II) nitrate (99.9%) was purchased from J. T. Baker. All solvents were used as received without further purification unless otherwise noted. Tetrabutylammonium perchlorate (TBAP) was recrystallized three times from ethyl acetate.

The syntheses of cis-dichlorobis(2,2′-bipyridine)ruthenium(II) (e.g., [Ru(bpy)$_2$Cl$_2$]),[23] 2,2′-bipyridyl-4,4′-dicarboxylic acid chloride (bpy(COCl)$_2$),[24] Fmoc-aeg(bpy)-O*t*Butyl,[19a] Fmoc-aeg(bpy)-COOH[19a] and Fmoc-aeg(ac)-OtButyl[19b] monomers, [Ru(bpy)$_2$(bpy[aeg-(bpy)-OtButyl]$_2$)](NO$_3$)$_2$ (e.g., **Ru-1**)[20a] and [**(Ru-1)-Cu**](PF$_6$)$_4$[20a] were performed and the products characterized as previously reported.

Oligopeptide Syntheses. Amine and Acid Deprotection. Fmoc deprotection was accomplished using a modified literature procedure.[25] Briefly, a sample of Fmoc-protected oligopeptide was stirred overnight with 1 mol equiv 1,8-diazabicyclo[5.4.0]undec-7-ene (DBU) and 10 mol equiv decane thiol in THF. After this time, the solvent was removed by rotary evaporation and the product redissolved in 75 mL of 0.15 M HCl. The aqueous solution was extracted 5 times with 50 mL hexanes, the organic layers were combined and back-extracted with 0.15 M HCl and all aqueous portions combined. The acidic aqueous solution was adjusted to a pH of 9−10 with saturated Na_2CO_3 and the aqueous layer extracted 5 times with 50 mL CH_2Cl_2, the organic fractions combined and dried with Na_2SO_4. Dichloromethane was removed by rotary evaporation to give the pure amine-terminated oligopeptide. In each case, removal of the Fmoc was confirmed by mass spectrometry and by noting the absence of Fmoc proton peaks in the aromatic region of the ^{1}H NMR spectra.

Cleavage of the *tert*-butyl protecting groups from select oligopeptides to form terminal carboxylic acids was accomplished by acid hydrolysis in a 25/75 (v/v) trifluoroacetic acid/dichloromethane solution. The solution was stirred for 4 h and the solvent removed by rotary evaporation. Diethyl ether was added to precipitate a pale-yellow solid. The ether was decanted and the solid was dried by vacuum to give the pure carboxylic acid-terminated oligopeptide. In each case, removal of the *t*-butyl was confirmed by the absence of the proton peaks of the *t*-butyl group in the ^{1}H NMR spectrum.

NH$_2$-[aeg(bpy)]-O^{t}Butyl (1). The Fmoc-protected bpy-substituted aeg monomer (Fmoc-aeg(bpy)-O*t*Butyl)[19a] was synthesized as previously reported. The Fmoc protecting group removed and the product isolated as described above, giving 1.20 g of solid (85% yield). ^{1}H NMR, 300 MHz, $CDCl_3$: 1.38 (s, 9H); 2.36 (s, 3H); 2.78 (t, 2H); 3.37−3.43 (t-t, 2H); 3.65 (d, 2H); 3.91 (d, 2H); 7.05 (d, 1H); 7.23 (dd, 1H); 8.15 (s, 1H); 8.22 (d, 1H); 8.45 (d, 1H); 8.55 (d, 1H). MS (ESI$^+$) [M + H$^+$] Calc: 385.2; Found: 385.2.

NH$_2$-[aeg(ac)-aeg(bpy)]-O^{t}Butyl (2). The acid terminus of the Fmoc-aeg(ac)-O^{t}Butyl monomer was deprotected as described above, and 5.04 g of the product (Fmoc-aeg(ac)-COOH, 16 mmol)

(22) (a) Saini, S.; Srinivas, G.; Bagchi, B. *J. Phys. Chem. B* **2009**, *113*, 1817–1832. (b) Davis, W. B.; Wasielewski, M. R.; Ratner, M. A.; Mujica, V.; Nitzan, A. *J. Phys. Chem. A* **1997**, *101*, 6158–6164.

(23) Sullivan, B. P.; Salmon, D. J.; Meyer, T. J. *Inorg. Chem.* **1978**, *17*, 3334–3341.

(24) Ko, C. C.; Wu, L. X.; Wong, K.; Zhu, N.; Wing-Wah Yam, V. *Chem.—Eur. J.* **2004**, *10*, 766–776.

(25) Sheppeck, J. E.; Kar, H.; Hong, H. *Tetrahedron Lett.* **2000**, *41*, 5329–5333.

was dissolved in 600 mL CH_2Cl_2 with 4.58 g HBTU (16 mmol), 2.01 g HOBT (16 mmol) and 19.6 mL diisopropylethylamine (DIPEA, 112 mmol), and stirred for 15 min at 0 °C. A 3.76 g amount of H_2N-aeg(bpy)-O^{t}Butyl (**1**, 9.78 mmol) was added to the solution and stirred overnight at room temperature. Solvent was removed by rotary evaporation, and the pale-yellow residue was purified by column chromatography with silica gel using 5/95 (v/v) CH_3OH/CH_2Cl_2 to give 2.46 g (33.5%) of the Fmoc-protected dipeptide **2**. ^{1}H NMR, 360 MHz, $CDCl_3$: 1.42 (d, 9H); 2.01 (d, 3H); 2.38 (d, 3H); 3.22−3.54 (m-m, 7H); 3.54−3.64 (m, 1H); 3.66 (s, 1H); 3.79−4.03 (s-s, 4H); 4.15 (m, 1H); 4.32 (d, 2H); 7.08 (t, 1H); 7.15−7.27 (m, 3H); 7.27−7.38 (m, 3H); 7.53 (t, 2H); 7.70 (d, 2H); 8.18 (t, 2H); 8.44 (d, 1H); 8.57, (m, 1H). MS (ESI$^+$) [M + H$^+$] Calc: 749.4; Found: 749.5. The Fmoc was cleaved and dipeptide **2** isolated as described above; a 1.42 g amount of the pure product was collected (82% yield). ^{1}H NMR, 360 MHz, $CDCl_3$: 1.39 (d, 9H); 1.94 (d, 3H); 2.37 (s, 3H); 3.31−3.52 (m-m, 10H); 3.82 (d, 2H); 3.90 (d, 2H); 4.02 (s, 1H); 7.08 (s, 1H); 7.21 (m, 1H); 8.14 (m, 2H); 8.43 (d, 1H); 8.54 (s, 1H). MS (ESI$^+$) [M + H$^+$] Calcd: 527.6; Found: 527.4.

NH_2-[(aeg(ac))$_2$-aeg(bpy)]-O^{t}Butyl (3). To 1 L of CH_2Cl_2 were added 7.15 g of Fmoc-aeg(ac)-COOH (18.7 mmol), 6.52 g of HBTU (18.7 mmol), 2.86 g of HOBT (18.7 mmol) and 38 mL of DIPEA (221 mmol), which was stirred at 0 °C for 15 min. A 6.56 g amount of H_2N-aeg(ac)-aeg(bpy)-O^{t}Butyl (**2**, 12.5 mmol) was added, and the mixture was stirred overnight. Solvent was removed and the crude residue was purified with column chromatography on silica using 9/95 (v/v) CH_3OH/CH_2Cl_2: a 3.78 g (34% yield) amount of the Fmoc-protected tripeptide was obtained. ^{1}H NMR, 400 MHz, $CDCl_3$: 1.41 (d, 9H); 1.99 (m-m, 6H); 2.37 (s, 3H); 3.22−3.70 (m-m, 14H); 3.72−4.06 (m-m, 6H); 4.06−4.37 (m-m, 3H); 7.09 (t, 1H); 7.16 (m, 1H); 7.25 (m, 3H); 7.33 (m, 2H); 7.38−7.58 (m-d, 3H); 7.70 (d, 2H); 7.94−8.23 (m-m, 3H); 8.44 (m, 1H); 8.55 (m, 1H). MS (ESI$^+$) [M + H$^+$] Calcd: 892.0; Found: 891.7. The Fmoc protecting group was cleaved and tripeptide **3** isolated and purified as described above, yielding 2.13 g (75% yield) of the pure compound. ^{1}H NMR, 360 MHz, $CDCl_3$: 1.43 (d, 9H); 1.93−2.17 (m-m, 6H); 2.41 (s, 3H); 3.26−3.53 (m-m, 11H); 3.57 (m, 2H); 3.68 (d, 1H); 3.74−4.07 (m-m, 6H); 7.11 (s, 1H); 7.25 (m, 3H); 8.20 (m, 2H); 8.47 (s, 1H); 8.59 (s, 1H). MS (ESI$^+$) [M + H$^+$] Calcd: 669.8; Found: 669.6.

NH_2-[aeg(bpy)]$_2$-O^{t}Butyl (4). To 250 mL of CH_2Cl_2 were added 4.37 g of Fmoc-aeg(bpy)-COOH (7.95 mmol), 3.02 g of HBTU (7.97 mmol), 1.22 g of HOBT (7.95 mmol), and 9.0 mL of DIPEA (53 mmol), and the mixture was stirred for 15 min at 0 °C. A 2.41 g amount of H_2N-aeg(bpy)-O^{t}Butyl (**1**, 6.28 mmol) was added, and the solution was stirred for 3 days at room temperature. Solvent was removed, and the crude residue was purified by column chromatography with silica using 5/95 (v/v) CH_3OH/CH_2Cl_2 to yield 3.20 g of the Fmoc-protected product (43.9% yield). ^{1}H NMR, 360 MHz, $CDCl_3$: 1.41 (d, 9H); 2.37 (m, 6H); 3.22−3.74 (m-m 10H); 3.74−4.12 (m-m, 6 H); 4.12−4.41 (m-m, 3H); 7.04 (m, 2H); 7.10−7.38 (m-m, 7H); 7.43 (m, 1H); 7.54 (t, 2H); 7.70 (m, 2H); 8.16 (m, 4H); 8.32−8.61 (d-m, 4H). MS (ESI$^+$) [M + H$^+$] Calcd: 917.4; Found: 917.7. The Fmoc group was cleaved and 2.45 g of dipeptide **4** isolated as described above, yielding 1.55 g (82%), ^{1}H NMR, 400 MHz, $CDCl_3$: 1.40 (m, 9H); 2.37 (d, 6H); 3.27−3.57 (m-m, 7H); 3.57−3.72, 3H); 3.72−4.07, 7H); 7.00−7.20 (m-m, 3H); 8.02−8.31 (m-m, 5H); 8.32−8.58 (m-m, 4H). MS (ESI$^+$) [M + H$^+$] Calcd: 695.4; Found: 695.5.

NH_2-[aeg(bpy)-aeg(ac)-aeg(bpy)]-O^{t}Butyl (5). A 2.30 g amount of Fmoc-aeg(bpy)-COOH (4.18 mmol) was combined with 1.62 g of HBTU (4.18 mmol), 0.66 g of HOBT (4.18 mmol), and 4.0 mL of DIPEA (18 mmol) in 250 mL CH_2Cl_2, and the mixture was stirred for 15 min at 0 °C. A 1.52 g amount of H_2N-aeg(AC)-aeg(bpy)-O^{t}Butyl (**3**, 2.89 mmol) was added to the solution, which was stirred for 3 days at room temperature. Solvent was removed, and the crude residue was purified by column chromatography silica using 5/95 (v/v) CH_3OH/CH_2Cl_2 to yield 1.21 g of the Fmoc-protected tripeptide (40% yield). ^{1}H NMR, 400 MHz, $CDCl_3$: 1.41 (d, 9H); 1.99 (m, 3H); 2.37 (s, 6H); 3.22−3.74 (m-m, 14H); 3.74−4.12 (m-m, 8H); 4.12−4.41 (m-m, 3H); 7.07 (m, 2H); 7.12−7.38 (m-m, 7H); 7.40 (m, 1H); 7.47 (t, 1H); 7.54 (d, 2H); 7.69 (m, 2H); 8.15 (m, 4H); 8.31−8.59 (m-m, 4H). MS (ESI$^+$) [M + H$^+$] Calcd: 1059.22; Found: 1059.7. Following the standard procedure above, the Fmoc was cleaved and tripeptide **5** was isolated, giving 0.805 g (85% yield). ^{1}H NMR, 360 MHz, $CDCl_3$: 1.40 (m, 9H); 1.98 (m, 3H); 2.38 (s, 6H); 3.25 (t, 2H); 3.29−3.58 (m-m, 12H); 3.64 (m, 2H); 3.82 (d, 2H); 3.85−4.05 (m-m, 6H); 7.08 (d, 2H); 7.14−7.30 (m-m, 2H); 8.17 (d, 4H); 8.44 (d, 2H); 8.54 (d, 2H). MS (ESI$^+$) [M + H$^+$] Calcd: 837.4; Found: 837.7.

General Approach for Ru Hairpin Complex Syntheses. Starting with the heteroleptic Ru complex $[Ru(bpy)_2(bpy(COOMe)_2)]^{2+}$,[26] this was converted to the dicarboxylic acid complex ($[Ru(bpy)_2(bpy(CO_2H)_2)]^{2+}$)[27] by base hydrolysis with 2 M NaOH followed by acidification with conc. HCl. The product was refluxed in 50 mL CH_2Cl_2 and 2 mL $SOCl_2$ overnight to form the diacid chloride complex, $[Ru(bpy)_2(bpy(COCl)_2)]^{2+}$. The solution was cooled to room temperature and filtered to give a red solid which was washed with cold, dry CH_2Cl_2 and used immediately. To form the Ru hairpin complexes, the $[Ru(bpy)_2(bpy(COCl)_2)]^{2+}$ was combined with ∼ 8 mol equiv of amine-terminated oligopeptide (**1**−**5**) and 2 mL triethylamine in 50 mL dry CH_2Cl_2. The reaction was stirred overnight at room temperature and the solvent removed by rotary evaporation. The remaining red residue was purified first by column chromatography with alumina using a 10/90 (v/v) CH_3OH/CH_2Cl_2 mobile phase. The first red band was collected and further purified on silica 5:4:1 (volume ratio) CH_3OH:H_2O:sat KNO_3 (aq) solution. In all cases, the products are isolated using previously reported methods[20a] and characterized as below:

$[Ru(bpy)_2(bpy([aeg(ac)-aeg(bpy)-OtButyl])_2)](NO_3)_2$ (Ru-2). The isolated product was an 0.099 g amount of red solid (68% yield). ^{1}H NMR, 400 MHz, CD_2Cl_2: 1.40 (m, 18H); 2.00 (m, 6H); 2.38 (s, 6H); 3.21−3.76 (m-m, 18H); 3.76−4.21 (d-d, 10H); 7.04−7.33 (s-s, 4H); 7.40 (m, 5H); 7.60−8.10 (m-m, 13H); 8.19 (m,4H); 8.48 (m, 8H); 8.97−9.51 (m-m, 4H). HR MS (ESI$^+$) [M^{2+} + NO_3^-] Calcd: 1736.6377; Found: 1736.6498. Elemental Anal. [**Ru-2** • CH_2Cl_2] Calcd: 55.47 C; 5.24 H; 14.87 N. Found: 55.59 C; 5.17 H; 14.91 N.

$[Ru(bpy)_2(bpy([(aeg(ac))_2-aeg(bpy)-OtButyl])_2)](NO_3)_2$ (Ru-3). A 280 mg amount of the product (51% yield) was isolated. ^{1}H NMR, 400 MHz, CD_2Cl_2: 1.40 (m, 18H); 1.80−2.11 (m-m, 12H); 2.39 (s, 6H); 3−16−3.74 (m-m, 26H); 3.74−4.15 (m-m, 14H); 7.11 (m, 2H); 7.19 (d, 1H); 7.27 (s, 1H); 7.43 (s, 5H); 7.57−8.11 (m-m, 14H); 8.21 (m, 5H); 8.42 (m, 3H); 8.50 (m, 6H); 8.91−9.52 (m-m, 4H). HR MS (ESI$^+$) [M^{2+}] Calcd: 979.9009; Found: 979.8941. Elemental Anal. **Ru-3** • 1 CH_2Cl_2 Calcd: 54.84 C; 5.49 H; 15.50 N. Found: 54.53 C; 5.56 H; 15.18 N.

$[Ru(bpy)_2(bpy([aeg(bpy)]_2-OtButyl)_2)](NO_3)_2$ (Ru-4). The reaction yielded a 539 mg amount of product (72% yield). ^{1}H NMR, 400 MHz, CD_2Cl_2: 1.37 (m, 18H); 2.20 (m, 4H); 2.32 (m, 8H); 3.21−3.98 (m-m, 28H); 3.98−4.35 (m, 6H); 6.92−7.27 (m, 8H); 7.37 (s, 4H); 7.60 (s, 3H); 7.72 (s, 4H); 7.79−8.02 (m, 8H); 8.02−8.55 (m, 19H); 8.93−9.49 (m, 3H). HR MS (ESI$^+$) [M^{2+}] Calcd: 1005.3947; Found: 1005.3943. Elemental Anal. **Ru-4** • 1.67 CH_2Cl_2 Calcd: 57.85 C; 5.11 H; 14.76 N. Found: 58.07 C; 5.10 H; 14.78 N.

$[Ru(bpy)_2(bpy[aeg(bpy)-aeg(ac)-aeg(bpy)-OtButyl)_2)](NO_3)_2$ (Ru-5). A total of 183 mg of **Ru-5** (74% yield) was obtained. ^{1}H NMR, 400 MHz, CD_2Cl_2: 1.41 (m, 18H); 1.87−2.12 (m, 6H); 2.27 (d, 4H); 2.39 (s, 8H); 3.19−3.64 (m, 20H); 3.64−3.80 (m, 8H); 3.83 (s, 3H); 3.86−4.01 (m, 7H); 4.01−4.23 (m, 6H); 7.01−7.30

(26) Martre, A.; Laguitton-Pasquier, H.; Deronzier, A.; Harriman, A. *J. Phys. Chem. B* **2003**, *107*, 2684–2692.
(27) Uppadine, L. H.; Keene, F. R.; Beer, P. D. *J. Chem. Soc., Dalton Trans.* **2001**, 2188–2198.

(m-m, 8H); 7.44 (t, 4H); 7.67 (s, 2H); 7,71−7.92 (m-m, 8 H); 7.92−8.10 (m, 6H); 8.11−8.60 (m-m, 20H); 8.92−9.52 (m-m, 4H). HR MS (ESI$^+$) [M^{2+}] Calcd: 1147.4690; Found: 1147.4626. Elemental Anal. **Ru-5** • 1.5 CH_2Cl_2 Calcd: 57.30 C; 5.34 H; 15.40 N. Found: 57.43 C; 5.34 H; 15.44 N.

Synthesis of Ruthenium−Copper Complexes. To prepare heterometallic samples for analysis, the standard procedure was to first dissolve a known quantity of Ru-oligopeptide complex in water. For complexes **Ru-2** and **Ru-3,** a 1.2 mol equiv amount of Cu^{2+} (from ∼50 mM $Cu(NO_3)_2$ (aq)) was added, and the resulting solution was stirred for two hours. For complexes **Ru-4** and **Ru-5**, 1 mol equiv amount of $Cu(NO_3)_2$ (aq) was added, and the solution was stirred for one hour; an additional 1.1 mol equiv were then added, and the solution was stirred for an hour.

In all cases, the product was isolated by addition of an aqueous saturated solution of NH_4PF_6, which immediately formed a red-brown solid that was collected on a medium frit and washed with water (3 × 15 mL) and diethyl ether (5 × 15 mL) to give the hetermometallic complex. Identity and purity of these compounds were determined by mass spectrometry and elemental analysis. [**Ru-2(Cu)**]$(PF_6)_4$ MS (ESI$^+$) [M^{4+} + 2PF_6^-] Calcd: 1013.7; Found: 1013.7. [M^{4+} + 1PF_6^-] Calcd 627.5; Round 627.5. Elemental Anal. Calc: 4.36 Ru; 2.74 Cu. Found: 4.50 Ru; 2.95 Cu. [**Ru-3(Cu)**]$(PF_6)_4$ MS (ESI$^+$) [M^{4+} + 2 PF_6^-] Calcd, 1155.8; Round, 1155.9. [M^{4+} + 1 PF_6^-] Calc: 722.2; Found: 722.2. [M^{4+}] Calcd: 505.4; Found: 505.4. Elemental Anal. **[Ru-3(Cu)]**$(PF_6)_4$ Calcd: 3.88 Ru; 2.44 Cu; Found: 3.65 Ru; 2.57 Cu. [**Ru-4(Cu)$_2$**]$(PF_6)_6$ MS (ESI$^+$) [M^{6+} + 4PF_6^-] Calcd: 1359.3; Found: 1359.3. [M^{6+} + 3PF_6^-] Calcd, 857.8; Found, 857.9. [M^{6+} + 2PF_6^-] Calcd: 607.1; Found: 607.2. [M^{6+} + 1PF_6^-] Calcd: 456.7; Found: 456.8. [M^{6+}] Calcd: 356.4; Found: 356.5. Elemental Anal. [**Ru-4(Cu)$_2$**]$(PF_6)_6$ Calcd: 3.36 Ru; 4.22 Cu. Found: 3.45 Ru; 4.50 Cu. [**Ru-5(Cu)$_2$**]$(PF_6)_6$ MS (ESI$^+$) [M^{6+} + 4PF_6^-] Calcd: 1501.3; Found: 1501.4. [M^{6+} + 3PF_6^-] Calcd: 952.6; Found: 952.6. [M^{6+} + 2PF_6^-] Calcd: 678.2; Found: 678.2. [M^{6+} + 1PF_6^-] Calcd: 513.6; Found: 513.6. [M^{6+}] Calcd: 403.8; Found: 403.8. Elemental Anal. [**Ru-5(Cu)$_2$**]$(PF_6)_6$ •NH_4PF_6 Calcd: 2.92 Ru; 3.68 Cu; Found: 2.82 Ru; 3.55 Cu.

Methods. UV−visible absorbance spectra were obtained with a double-beam spectrophotometer (Varian, Cary 500). Emission spectra were measured using a Photon Technology International (PTI) fluorescence spectrometer using an 814 photomultiplier detection system. Time resolved emission decays were measured following excitation using a N_2 dye laser (PTI model GL-302), averaging 16 decays with a 50 μs collection time per point. In variable temperature experiences, temperature was controlled using a constant temperature bath and flow-through cell housing and measured using a thermocouple adhered on the outer surface of the quartz cuvette. Samples were allowed to equilibrate each at temperature for a minimum of 10 min (with stirring) prior to measurement. Quantum yields and radiative and nonradiative decay rates[28] at all temperatures were determined using samples from which oxygen had been using removed in repetitive freeze−pump−thaw cycles, and finally measured in a sealed cell under nitrogen. Quantum yields were determined using the relationship:[29]

$$\Phi = \Phi_{ref}\frac{(I/A)}{(I_{ref}A_{ref})}\left(\frac{\eta}{\eta_{ref}}\right)^2 \quad (1)$$

where Φ is the radiative quantum yield of the sample; Φ is the known quantum yield of [Ru(bpy)$_3$]$^{2+}$ in acetonitrile = 0.062;[30] I is the integrated emission, A is the absorbance at the excitation wavelength; and η is the dielectric constant of the solvent, which is assumed to be the same for the acetonitrile solutions of sample and reference. The rates of radiative (k_r) and nonradiative (k_{nr}) decay were determined using the measured excited state lifetime (τ) and the equations:[28]

$$\tau^{-1} = k_r + k_{nr} \quad (2)$$

$$\Phi = \frac{k_r}{k_r + k_{nr}} \quad (3)$$

Spectrophotometric emission titrations were conducted in CH_3CN solutions at room temperature in the presence of air using known concentrations of Ru compounds. The compounds were excited at their MLCT absorbance maxima (λ_{ex} = 469 nm) and monitored at their emission maxima (λ_{em} = 650 nm). Spectra were obtained after stirring the solution with each known volumes (2−15 μL) of standard Cu^{2+} solutions (2−4 mM) in CH_3CN for 15 min.

Mass spectrometric analysis was performed on a Waters LCT Premier time-of-flight (TOF) mass spectrometer at the Penn State Mass Spectrometry Facility. Samples were introduced into the mass spectrometer using direct infusion via a syringe pump built into the instrument. The mass spectrometer was set to scan from 100−2500 *m/z* in positive ion mode using electrospray ionization (ESI).

NMR spectra were collected using either a 360 or 400 MHz spectrometers (Bruker) in the Lloyd Jackman Nuclear Magnetic Resonance Facility. Elemental analysis was performed by Galbraith Industries, with replicate analysis of all metal ratios in the heterometallic structures.

All electrochemical measurements were obtained using a CH Instruments potentiostat (Model 660) with 0.31 cm diameter glassy carbon working and Pt wire counter electrodes with a Ag quasi reference electrode. Solutions were prepared from distilled CH_3CN containing 0.2 M TBAP supporting electrolyte; the solutions were deoxygenated by purging with solvent-saturated N_2. Potentials are reported vs a saturated calomel electrode reference scale using ferrocene as an internal potential reference standard.

Results and Discussion

Synthesis of Oligopeptides. Our earlier report of aeg-substituted [Ru(bpy)$_3$]$^{2+}$ complexes used amide coupling chemistry to link a bpy-substituted aeg monomer to the Ru complex, and left the chain termini ester-protected.[20a] In principle, cleavage of the esters to produce terminal acid groups could be used to then extend the chains via sequential coupling of additional monomeric units. Our attempts to use this approach to synthesize the dipeptide-containing Ru complexes resulted in only very small reaction yields, and an alternative route that prepares and attaches the full-length oligpeptide was instead used. Scheme 2 contains the synthetic steps to synthesize the series of di- and tripeptides used in these experiments. Deprotection of either the acid or amine termini is accomplished using the same reagents as solid phase peptide synthesis, but requires isolation from the solution mixture prior to further reaction. Following selective deprotection of the monomers, dipeptides were synthesized using standard peptide coupling reagents. For example, reaction of H_2N-aeg(bpy)-O^{t}Butyl (**1**) with Fmoc-aeg(bpy)-COOH with HBTU, HOBT, and DIPEA produced Fmoc-protected dipeptide **4** in 43.9% yield. Analogous reaction of **1** with Fmoc-aeg(ac)-COOH gave Fmoc-protected dipeptide **2** in 33.5% yield. As shown in Scheme 2, the Fmoc group was cleaved from dipeptide **2** and its terminal amine was further coupled with either Fmoc-aeg(ac)-COOH or Fmoc-aeg(bpy)-COOH to afford tripeptides **3** and **5** in 34 and 40% yield, respectively. In each case, synthesis of the di- and tripeptides required more time because of the necessary intermediate purification steps, however the desired materials were made in

(28) Meyer, T. J. *Pure Appl. Chem.* **1986**, *58*, 1193–1206.
(29) Williams, A. T. R.; Winfield, S. A.; Miller, J. N. *Analyst* **1983**, *108*, 1067–1071.
(30) Lu, W.; Chan, M. C. W.; Zhu, N.; Che, C. M.; Li, C.; Hui, Z. *J. Am. Chem. Soc.* **2004**, *126*, 7639–7651.

Scheme 2. Synthetic Steps toward Di and Tripeptides[a]

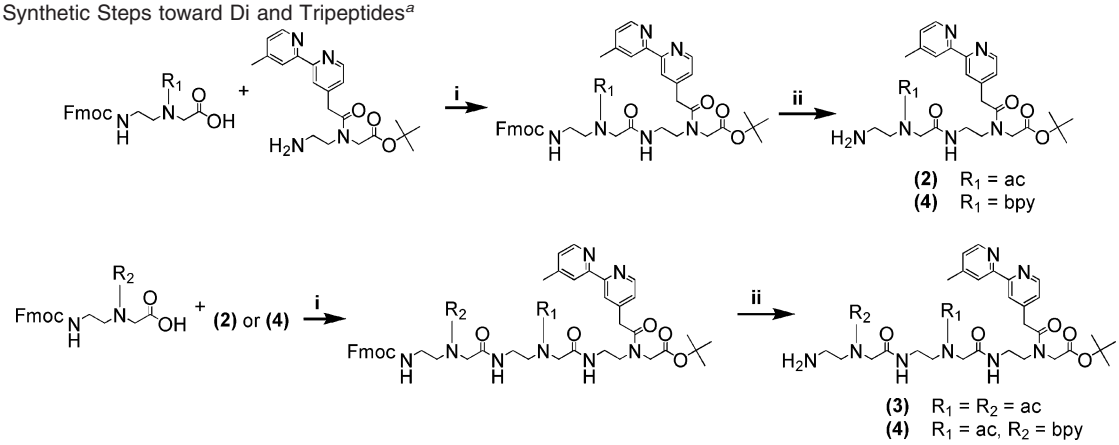

[a] (i) HBTU, HOBT, DIPEA, CH_2Cl_2, overnight; (ii) DBU, octanethiol, tetrahydrofuran, overnight.

gram scale quantities that are not readily achievable with solid-phase peptide synthetic methods. The purity and identity of the oligopeptides were confirmed by ^{1}H NMR spectroscopy and mass spectrometry, respectively.

Synthesis of Ru Complexes. Ruthenium hairpin complexes **Ru-2**, **Ru-3**, **Ru-4** and **Ru-5** were synthesized by reaction of an excess of amine-terminated di- or tripeptide with $[Ru(bpy)_2(bpy(COCl)_2)]^{2+}$ with triethyl amine in dry dichloromethane. This approach rapidly enabled yields of >50% in hundreds of mg scales. Molecular ion peaks observed in the electrospray mass spectra conclusively identified the products. Purity of these compounds was assessed by ^{1}H NMR spectroscopy (Supporting Information) and elemental analysis. NMR spectra confirmed the expected relative integrations of protons for the disubstituted Ru complexes; elemental analyses revealed the tendency to retain small amounts of solvent even after extensive drying. Slight differences between the theoretical and observed mass percentages of C, H and N, which are likely the result of residual salt (KNO_3) from the final purification column.

Analysis of the redox properties of the Ru complexes was performed using cyclic voltammetry. Figure 2 contains a cyclic voltammogram of an acetonitrile solution of **Ru-2** (black line), which is representative of the series of Ru complexes in that each has a reversible one-electron oxidation at ~1.3 V that is due to the metal centered $Ru^{III/II}$ couple. Three one-electron reductions are observed in the voltammogram, which are assigned to ligand-centered reductions of the $[Ru(bpy)_3]^{2+}$ core. The first of these appears at −1.27 V, and is due to the reduction of the diamide-substituted bpy ligand (e.g., $[Ru(bpy)(bpy(aeg)_2)] \rightarrow [Ru(bpy)(bpy^{\bullet-}(aeg)_2)]$), which is shifted to more positive potentials than the other two bpy ligands in the complex because of the electron withdrawing nature of the amides. Reductions of the other two ligands appear at ~−1.65 and −1.9 V, and are accompanied with a small amount of chemical irreversibility, as evidenced by the new (but small) oxidative peaks (~−0.15 V) during the return scans. We do not observe separate reduction waves associated with uncoordinated bipyridine ligands, consistent with the voltammogram of the bpy monomer (red line); these are outside the scanned potential window at larger overpotentials (Figure S17, Supporting Information). These data are summarized in Table 1 and exhibit only very minor differences in the redox couples across the five Ru complexes, reflective of their similar central structure.

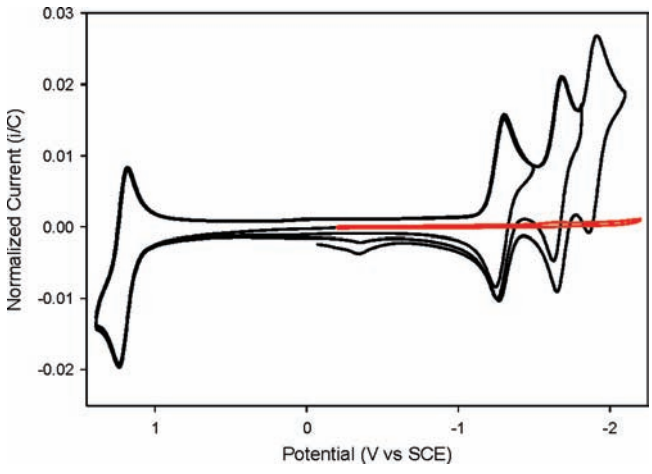

Figure 2. Cyclic voltammograms of acetonitrile solutions containing 1.09 mM **Ru-2** (black line) or 5.09 mM Fmoc-aeg(bpy)-O*t*Butyl (red line) with 0.2 M tetrabutylammonium perchlorate supporting electrolyte, obtained using a 0.068 cm^2 area glassy carbon working electrode and a potential scan rate of 75 mV/s. Currents are normalized to concentration.

Absorbance and emission spectra were also measured for each of the Ru complexes in acetonitrile solutions. In Table 1, each of the complexes has an absorbance band with a peak ~469 nm that is a result of the well-known metal-to-ligand charge transfer band of $[Ru(bpy)_3]^{2+}$.[31] The extinction coefficients (ϵ) and peak maxima do not vary as a function of the pendant aeg strands in the series of Ru complexes. In solutions that are thoroughly degassed, the quantum yields and peak wavelengths of the emission band (following excitation at 469 nm) also do not significantly vary among the Ru complexes. Of central interest to our work is understanding the processes following photoexcitation of the Ru center by monitoring the transient emission at 650 nm following pulsed excitation. The emission transients of **Ru-1** through **Ru-5** (see Supporting Information) show that each has a monoexponential emission decay, indicative of a single species radiatively relaxing to the ground state. Slight differences in intensity for these decay curves reflect minor variation of the quantum yields (Table 1). Fits of these emission decay lines provide the excited state lifetimes, τ, which are given in Table 1 and are approximately the same for all of the complexes.

Ru−Cu Heterometallic Complexes. To understand the photophysical behaviors and characterize the heterometallic com-

(31) Kalyanasundaram, K. *Coord. Chem. Rev.* **1982**, *46*, 159–244.

Table 1. Photophysical and Electrochemical Data for Ru Hairpin Complexes

	Ru-1	Ru-2	Ru-3	Ru-4	Ru-5
$\lambda_{max,\ abs}$ (nm)[a] (ϵ, $M^{-1}\ cm^{-1} \times 1000$)	469 (13.4)	469 (13.6)	469 (13.5)	469 (13.3)	469 (13.4)
$\lambda_{max,\ em}$ (nm)[b]	650	650	650	650	650
Φ[c]	0.0405	0.0468	0.0434	0.0541	0.0506
τ[d] (μs)	1.18	1.16	1.12	1.21	1.20
$k_r \times 10^4$ (sec^{-1}) [e]	3.43	4.02	3.87	4.47	4.20
$k_{nr} \times 10^5$ (sec^{-1})[e]	8.12	8.19	8.54	7.80	7.88
$E°$ $Ru^{3+/2+}$ (V)[f]	1.29	1.29	1.29	1.28	1.28
$E°$ $Ru^{2+/1+}$ (V)[f]	−1.26	−1.27	−1.35	− 1.27	−1.27
$E°$ $Ru^{1+/0}$ (V)[f]	−1.65	−1.65	−1.54	−1.65	−1.63
$E°$ $Ru^{0/-1}$ (V)[f]	−1.88	−1.91	−1.99	−1.90	−1.89

[a] Maximum absorbance wavelength and extinction coefficient for the metal to ligand charge transfer band. [b] Peak emission wavelength following excitation at $\lambda_{max,abs}$. [c] Emission quantum yields following excitation at $\lambda_{max,abs}$, determined using eq 1 [Ru(bpy)$_3$]$^{2+}$ in CH_3CN (Φ = 0.062) as a reference.[30] [d] Excited state lifetime in dearated CH_3CN solutions, determined from the emission decay following pulsed excitation at $\lambda_{max,abs}$. [e] Rates of radiative (k_r) and nonradiative decay (k_{nr}) calculated using eq 2 and 3. [f] Reaction formal potentials vs SCE, measured in 0.2 M TBAP in dearated CH_3CN.

plexes, experiments were conducted with samples made at either the preparatory scale or studied as a function of added Cu^{2+} during spectrophotometric titrations. Bulk scale synthesis of ruthenium−copper complexes provided the material necessary for elemental analysis and mass spectrometry. A challenge for inorganic supramolecular analysis is the ionization of large and highly charged species, which presents difficulties especially when these contain labile metal ions. However, using softer ionization methods, we were able to obtain mass spectra for all of the heterometallic complexes. In each case, molecular ion peaks for species with charges ranging from +2 up to +6 were observed. For example in Figure 3, peaks corresponding to M^{2+}, M^{3+}, M^{4+}, M^{5+} and M^{6+} molecular ions were observed for the trimetallic **[Ru-5(Cu)$_2$]$^{6+}$** complex associated with decreasing numbers of PF_6^- anions. In comparison with the calculated isotopic splitting patterns expected for these species, these data conclusively identify the heterometallic complexes. (Series of molecular ion peaks for each of the heterometallic complexes are provided in Supporting Information.)

Elemental analysis was used to further characterize the multimetallic complexes: with the pure Ru complexes in hand, elemental analyses focused on the comparison of the relative amounts of Cu and Ru in the products. We had previously reported the Ru:Cu mole ratio in **Ru-1-(Cu)** to be 1: 0.99.[20] In the new dimetallic structures, the determined molar ratios of Ru:Cu in the **Ru-2(Cu)**, and **Ru-3(Cu)** complexes are 1 Ru: 0.96 Cu and 1 Ru: 1.11 Cu, respectively. In complexes **Ru-4(Cu)$_2$** and **Ru-5(Cu)$_2$** these values were found to be 1 Ru: 2.07 Cu and 1 Ru:2.00 Cu, respectively. These elemental analyses confirm that the isolated products contain the expected molar ratios of Ru and Cu for the pure heterometallic species, with minor differences between theoretical and experimental molar ratios of Ru and Cu that are most likely the result of solvent or salt.

Copper Coordination Emission Titrations. In Scheme 1, the structural variations were designed to probe the impact of the spacing and number of coordinated Cu^{2+} ions on the quenching of [Ru(bpy)$_3$]$^{2+}$ emission. Crystallization attempts are still ongoing in our laboratories, however for understanding the solution phase emission quenching dynamics, the metal−metal distances *in solution* are more germane. We therefore qualitatively consider the relative molecular structures and dynamics and compare these to observed spectroscopic results. In a fully extended (all-trans) aminoethylglycine chain (modeled using Hyperchem 6.0, and which has been described for peptide nucleic acid chains[32]), the (through space) distance between substituents (e.g., bpy or ac) is ~ 7 Å; we use this as an approximation of the distances between tethered metal complexes. [Note that the distance through-bond, using known bond lengths, is ~13 Å between substituents.] In solution, the aeg chains are most certainly flexible and the solution structures dynamic, so that the separation distance between metal centers is likely to vary. However, it is probable that the length of the oligopeptides and the charges of the metal complexes place some energetic restraints on this. In the case of **Ru-1**, the single aeg backbone unit is short and the Cu cross-link is relatively strained compared to the longer strands of **Ru-2** and **Ru-3**. As a result, the distance between Ru and Cu in **Ru-3** (~23 Å maximum) is expected to be larger than in **Ru-2** (~16 Å maximum) and **Ru-1** (~ 9 Å maximum), but to also vary more greatly because of the conformational dynamics of the longer, flexible tripeptide backbone. When additional metals cross-link the strands, for example, in **Ru-4** (Ru−Cu distance ~9 Å, Cu−Cu ~7 Å, maximum) and **Ru-5** (Ru−Cu ~9 Å, Cu−Cu ~14 Å, maximum), these are expected to somewhat limit the chain flexibility. Electrostatic repulsions of the +2 charged metal complexes would bias the structures toward more extended conformations but not completely limit the dynamic nature of the chains' motions. This qualitative picture is applied to the measured emission quenching and rates to understand the role of structure on photochemistry of the multimetallic complexes.

In complex **Ru-1**, coordination to a molar equivalent of Cu^{2+} ion resulted in 97% quenching of the photoemission of the Ru complex.[20a] Our interest in understanding the process by which this occurs led us to examine the role of the number and separation of Cu^{2+} ions bound by the Ru hairpin complexes. The emission spectra for Ru hairpin complexes following excitation at 469 nm are identical for the series of Ru complexes (for example see SI). In each case emission is initially bright but incremental addition of Cu^{2+} to the solution causes the emission intensity to decrease. In a control experiment, titration of [Cu(bpy)$_2$]$^{2+}$ into a solution containing [Ru(bpy)$_3$]$^{2+}$ (i.e., without an aeg linker) at identical concentrations, no quenching of the Ru emission is observed (Figure S16, Supporting Information) even after 5 mol equiv of Cu have been added. Figure 4A plots the spectrophotometric titration data for complexes containing a pair of free bipyridine ligands (e.g., **Ru-1**, **Ru-2**, and **Ru-3**), monitoring the emission intensity at λ_{em} = 650 nm following addition of Cu^{2+}. These data

(32) (a) Nielsen, P. E.; Haaima, G. *Chem. Soc. Rev.* **1997**, *26*, 73–78. (b) Rasmussen, H.; Kastrup, J. S.; Nielsen, J. N.; Nielsen, J. M.; Nielsen, P. E. *Nat. Struct. Biol.* **1997**, *4*, 98–101.

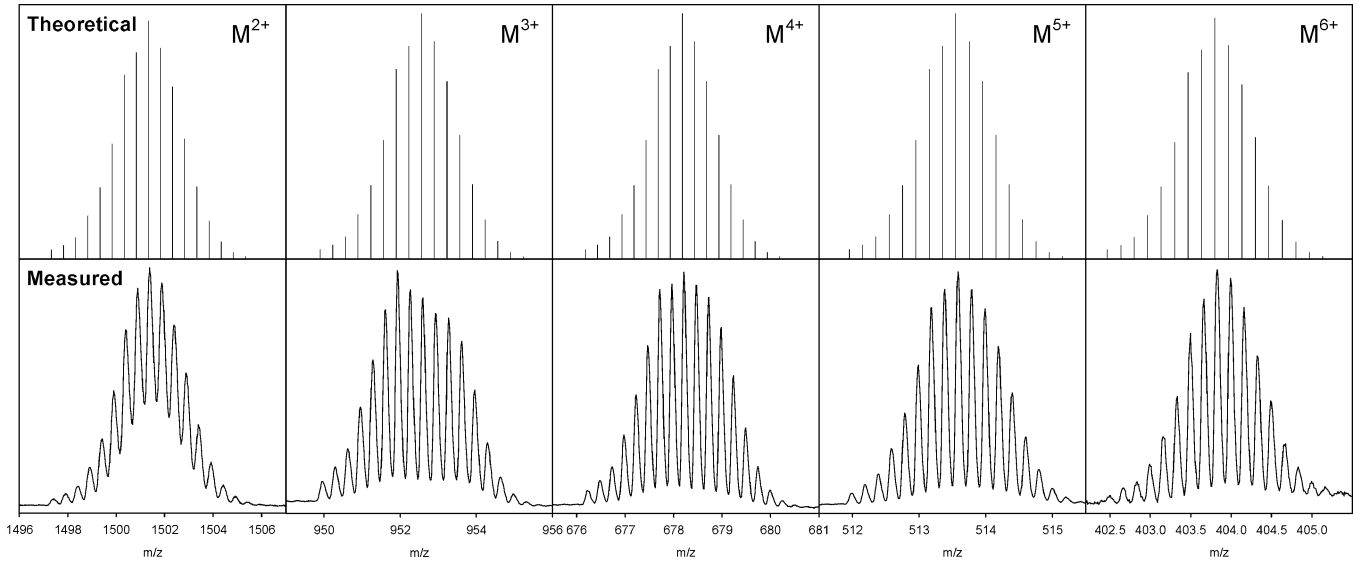

Figure 3. Molecular ion peaks observed by positive ion electrospray mass spectrometry, plotted together with the calculated mass and isotopic splitting patterns for $[\mathbf{Ru\text{-}5(Cu)_2}](PF_6)_6$.

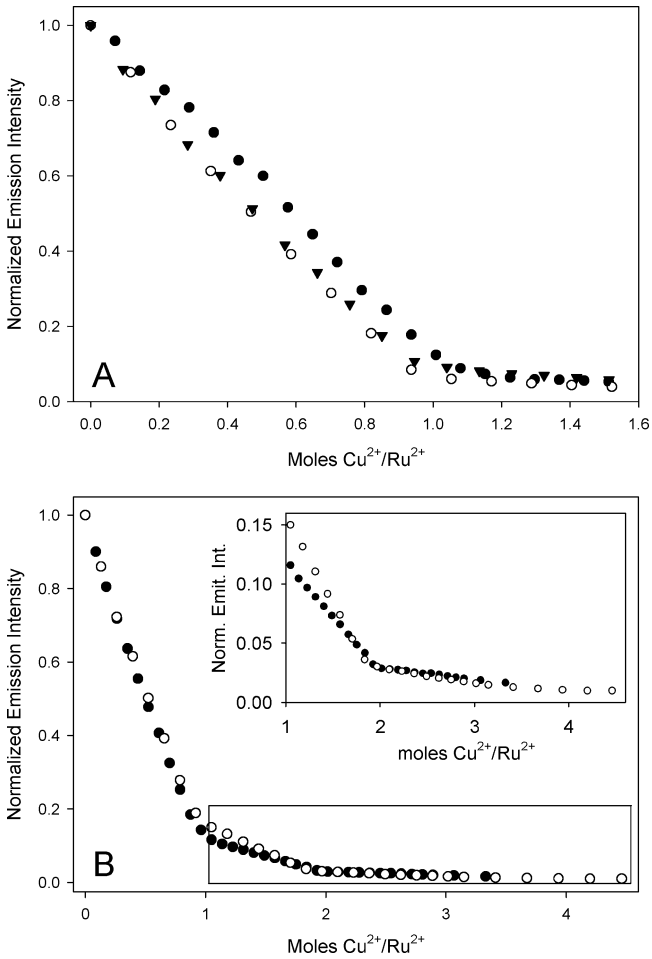

Figure 4. (A) Plot of emission intensity of CH_3CN solutions containing (•) 140 μM **Ru-1** with addition of 5 μL aliquots of 5.3 mM $Cu(NO_3)_2$; (○) 58.7 μM **Ru-2** with additions of 5 μL aliquots of 3.41 mM $Cu(NO_3)_2$; (▼) 104 μM**Ru-3** with additions of 5 μL aliquots of 4.86 mM $Cu(NO_3)_2$. (B) Plot of emission intensity of CH_3CN solutions of (•) 95.0 μM **Ru-4** and (○) 57.6 μM **Ru-5** after incremental additions of 7 μL of 2.83 mM $Cu(NO_3)_2$ and 5 μL of 3.86×10^{-3} mM $Cu(NO_3)_2$, respectively, versus the molar ratio of Cu^{2+} to Ru^{2+}. (Inset) Expanded region of the titration curve at higher Cu^{2+} concentrations.

reveal that for these complexes the emission intensity decreases with Cu^{2+} until reaching a stoichiometric point of [Cu] ≈ [Ru], after which the intensity levels and is constant. These molar ratios are consistent with the formation of the dimetallic complexes containing $[Cu(bpy)_2]^{2+}$ coordinative cross-links, and which are observed in the bulk-scale preparation, **Ru-1-(Cu)**, **Ru-2-(Cu)**, and **Ru-3-(Cu)**. The final intensities of the titration curves in Figure 4A (i.e., after the equivalence point) are similar for the three compounds, and correspond to quenching of the initial $Ru(bpy)_3$ emission by 97%, 95% and 90% in **Ru-1-(Cu)**, **Ru-2-(Cu)** and **Ru-3-(Cu)**, respectively. Differences in the quenching efficiency of the bound Cu^{2+} ion are attributed to the length of the oligopeptide, and the relative rates are quantitatively examined in thoroughly dearated solutions below.

Compounds **Ru-4** and **Ru-5** each contain four free bipyridine ligands that are available for Cu^{2+} binding to form $[Cu(bpy)_2]^{2+}$ cross-links. Metal binding stoichiometry was determined by the spectrophotometric emission titration as a function of $Cu(NO_3)_2$ added to the solution. In Figure 4B, the emission intensities of **Ru-4** and **Ru-5** (at 650 nm) are plotted versus the relative amount of added Cu^{2+}. A striking difference between these titration curves and those in Figure 4A (and reported previously[20a]) is that in both complexes the emission is quenched in two distinct phases. For both compounds, the intensity decreases until the Cu^{2+} concentration is equal to the Ru complex concentration, at which point the Ru emission is quenched by ∼84%, less than observed in **Ru-1**, **Ru-2**, and **Ru-3**. As more Cu^{2+} is added to **Ru-4** and **Ru-5**, so that [Cu] > [Ru], the emission intensity continues to decrease until ∼2 mol equiv of Cu^{2+} are in the solution (inset of Figure 4B). After 2 equiv of Cu^{2+} are injected, the emission is quenched by 97% for both **Ru-4** and **Ru-5**.

We attribute the two inflections of the titration curves in Figure 4B to the sequential binding of two Cu^{2+} ions each by **Ru-4** and **Ru-5**. As depicted in Figure 5, during the titration the first Cu^{2+} ion to bind can form $[Cu(bpy)_2]^{2+}$ by coordination with two of the four pendant bpy ligands (note that the close proximity on the backbone prevents bpy ligands on the same aeg chain from wrapping around the same metal ion).[19a] Our observations of Cu^{2+} binding by **Ru-1**, **Ru-2** and **Ru-3** suggest slightly different quenching efficiencies based on the location of the $[Cu(bpy)_2]^{2+}$ cross-link. The lower observed quenching efficiency of **Ru-4** and

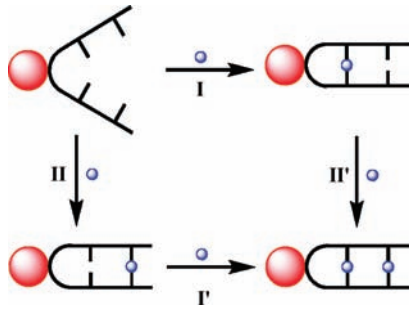

Figure 5. Depiction of the sequential binding of two Cu^{2+} ions (blue sphere) by **Ru-4** or **Ru-5** (red sphere).

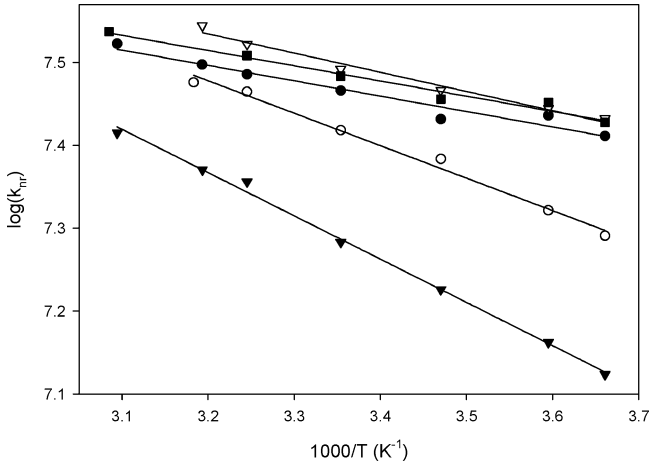

Figure 6. Arrhenius plot of the nonradiative relaxation rate (k_{nr}) for (•) 41 μM **Ru-1-(Cu)**; (○) 53 μM **Ru-2-(Cu)**; (▼) 40 μM **Ru-3-(Cu)**; (▽) 36 μM **Ru-4-(Cu)$_2$**; and (■) 17 μM **Ru-5-(Cu)$_2$** in deoxygenated CH_3CN solutions.

Ru-5 at one molar equivalent of Cu^{2+} is consistent with having a mixture of locations of the Cu^{2+} between the two dipeptide strands (i.e., via pathway I or II in Figure 5, or other possible isomers). Lability of the copper ion, together with further addition of Cu^{2+}, enables rearrangement and binding of a second metal ion (reaction I′ or II′ in Figure 5) and ultimate quenching efficiency of 97%. In both **Ru-4-(Cu)$_2$** and **Ru-5-(Cu)$_2$**, because the closest Ru−Cu distance is equivalent to that in the **Ru-1-(Cu)** dimetallic complex, the quenching efficiencies are approximately the same.

Time-Resolved Emission Spectroscopy. To obtain quantitative rate information about the process by which the Ru excited state is quenched, the solutions were carefully deoxygenated (by several cycles of freeze−pump−thaw) and the time-dependent emission decays and quantum yields were examined. The emission transients following an 800 ps excitation pulse were fit to monoexponential decays to give the excited state lifetimes listed in Table 2 for each of the heterometallic complexes. In comparison with monometallic **Ru-1**, the excited state lifetimes are ∼2 orders of magnitude shorter when Cu^{2+} is bound. Using solutions with known concentrations, the absorbance and integrated emission peaks were measured and used to determine the emission quantum yields (Table 2). Similar to the impact on lifetime, the quantum yields decrease drastically upon Cu^{2+} coordination.

Together with the quantum yields, the excited state lifetimes were used to determine the rate of radiative (k_r) and nonradiative (k_{nr}) relaxation. In **Ru-1**, the radiative and nonradiative relaxation rates are relatively similar in magnitude (∼10^5 s^{-1}). Addition of Cu^{2+} does not change the radiative relaxation rate but causes a ∼30-fold increase in the nonradiative relaxation rate, the latter of which is dependent on the number and location of the $[Cu(bpy)_2]^{2+}$ cross-links. For the dimetallic complexes, k_{nr} slightly decreases as the $[Cu(bpy)_2]^{2+}$ complex is moved farther away from the Ru center. Addition of a second Cu^{2+} to the complex slightly increases k_{nr}.

The temperature dependence of the relaxation rates following excitation in the series of complexes was also measured to begin to understand the dynamics in these systems. In all cases, the quantum yields and excited state lifetimes were measured as a function of temperature to accurately obtain the values of k_r and k_{nr}. Figure 6 contains the activation plots for the calculated values of k_{nr} for each of the heterometallic compounds; using the slopes of these lines, the activation energy (E_a) and intercepts (A) are determined (Table 2). For comparison, these data were also obtained for **Ru-1**, in which the excited state is long-lived and there is no bound $[Cu(bpy)_2]^{2+}$. Consistent with the trends observed for k_{nr}, E_a increases with the distance between Ru and Cu (e.g., **Ru-1-(Cu)**, **Ru-2-(Cu)** and **Ru-3-(Cu)**) yet the barriers for the trimetallic structures (e.g., **Ru-4-(Cu)$_2$** and **Ru-5-(Cu)$_2$**) are similar and approximately the same as in **Ru-1-(Cu)**. The intercepts are approximately the same for all of the heterometallic complexes, consistent with an intramolecular quenching mechanism that requires similar molecular rearrangements for the series of structures.

As is often the case with excited state quenching in donor−acceptor assemblies, quenching of the emissive Ru complex could occur by energy or electron transfer mechanisms or a combination of these.[17d,22] Experimentally distinguishing the contributions of these possible pathways is challenging, however the above data do offer some insight into these systems. The weak extinction coefficient of the $[Cu(bpy)_2]^{2+}$ complex makes energy transfer a possible but likely minor component of the excited state quenching.[20a,33] The favorable redox potentials of the excited state Ru complex ($E°$ $Ru^{3+/2+*} \approx -0.64$ V vs SCE)[34] and tethered Cu complexes ($E°$ $Cu^{2+/1+} = 0.04$ V vs SCE) make quenching by electron transfer an energetically favorable pathway ($\Delta G \approx -0.7$ eV),[7b] following the reaction:

$$[Ru^{III}(bpy)_2(bpy^{\bullet-})]^* - [Cu^{II}(bpy)_2] \rightarrow [Ru^{III}(bpy)_3] - [Cu^{I}(bpy)_2] \quad (4)$$

It is important to note that the electron donor and acceptor species are tethered by two aeg strands (indicated by the dash in eq 4), essentially holding them at locations that are expected to be close to the precursor state. In this quenching route, charge recombination by back electron transfer ($\Delta G \approx -1.2$ eV) would restore the ground state Ru(II) and Cu(II) complexes. In the heterometallic complexes, the measured k_{nr} are most likely dominated by the reaction in eq 4, since the rate constants increase by orders of magnitude in the complexes containing Cu^{2+}. Addition of a second bound Cu^{2+} to **Ru-4** and **Ru-5** slightly increases k_{nr}, which could be due to electron hopping between Cu centers (*vide infra*) or the impact of increased structural rigidity with the added metal cross-link. The latter of these would be expected to increase k_{nr} in either electron or energy transfer mechanism.

(33) (a) Baggott, J. E.; Billing, M. J. *J. Phys. Chem.* **1980**, *84*, 3012–3019. (b) Milosavljevic, B. H.; Thomas, J. K. *J. Chem. Soc. Faraday Trans.* **1985**, *81*, 735–744. (c) Geiber, B.; Alsfasser, R. *Eur. J. Inorg. Chem.* **1998**, 957–963. (d) Bolletta, B.; Costa, I.; Fabbrizzi, L.; Licchelli, M.; Montalti, M.; Pallavicini, P.; Prodi, L.; Zaccheroni, N. *J. Chem. Soc., Dalton Trans.* **1999**, 1381–1385. (e) Ajayakumar, G.; Sreenath, K.; Gopidas, K. R. *Dalton Trans.* **2009**, 1180–1186.
(34) Orellana, G.; Quiroga, M. L.; Braun, A. M. *Helv. Chim. Acta* **1987**, *70*, 2073–2086.

Table 2. Photophysical Data for Ru−Cu Heterometallic Complexes

	Ru-1	Ru-1-(Cu)	Ru-2-(Cu)	Ru-3-(Cu)	Ru-4-$(Cu)_2$	Ru-5-$(Cu)_2$
τ [a] (ns)	1180	34.3	38.0	51.5	32.0	32.7
Φ[a]	0.0405	0.00100	0.00168	0.00186	0.00119	0.0012
$k_r \times 10^4$ (sec^{-1})[a]	3.43	2.93	4.42	3.60	3.74	3.67
E_{a,k_r} (kJ/mol) [b]	2.76 ± 0.5	1.29 ± 0.4	10.6 ± 0.3	7.86 ± 0.6	3.9 ± 0.4	1.9 ± 0.3
log A_{k_r} [c]	5.1 ± 0.1	4.7 ± 0.1	6.5 ± 0.1	5.9 ± 0.1	5.3 ± 0.1	4.9 ± 0.01
$k_{nr} \times 10^7$ (sec^{-1}) [a]	0.081	2.91	2.62	1.93	3.14	3.05
$E_{a,k_{nr}}$ (kJ/mol) [b]	2.0 ± 0.5	3.5 ± 0.3	7.5 ± 0.4	10.0 ± 0.4	4.4 ± 0.3	3.5 ± 0.3
log $A_{k_{nr}}$ [c]	6.3 ± 0.1	8.1 ± 0.1	8.7 ± 0.1	9.0 ± 0.1	8.3 ± 0.1	8.1 ± 0.1

[a] Emission lifetime (τ), quantum yield (Φ), radiative and nonradiative (k_r and k_{nr}) rate constants at 25 °C in dearated CH_3CN solutions. [b] Activation energy, determined from the slopes of Arrhenius plots as in Figure 6. [c] Intercept of the activation plot, in s^{-1}.

The modular nature of the aeg backbone allows us to easily prepare a series of molecules with increasing separation between the electron donor and acceptor sites. While it is clear from these data that k_{nr} and the separation distance are inversely related, it is striking that this dependence is relatively shallow. That is, electron transfer via tunneling through-bond would predict an exponential relationship between k_{nr} and distance ($\propto \exp^{-r}$); energy transfer quenching would have an inverse distance dependence ($\propto r^{-6}$))-these are clearly not the case, even given the inexactly known and dynamic Ru−Cu separation in solution. It is possible that the quenching mechanism changes as distance increases;[33b] over this range of structures the similarity in measured rates is not suggestive of mechanistic changes. Further, as the Ru−Cu distance increases the slower k_{nr} is a function of the higher activation barriers and *not* changes in the pre-exponential term. Larger barriers as a function of distance are consistent with additional outer sphere contributions, including solvent and counterion reorganization, prior to either electron or energy transfer.[35] The comparable intercepts implies that any molecular rearrangements to bring the Ru and Cu complexes into the precursor state prior to quenching are similar for the series of complexes: this would require concerted motion of the Cu-complex-linked strands on a short time scale. The current molecules and experiments are unable to distinguish between molecular folding to enable short distance events and quenching over larger distances, but ongoing studies in our group aim to resolve this question.

In the trimetallic complexes, if quenching occurs by electron transfer to the nearest Cu, there is a also the smaller probability of directly reducing the more distal Cu^{2+} complex. In either case, an initial electron transfer step would result in formation of adjacent and mixed valent Cu complexes:

$$[Ru^{III}(bpy)_2(bpy^{\bullet-})]^* - [Cu^{II}(bpy)_2] - [Cu^{II}(bpy)_2] \rightarrow [Ru^{III}(bpy)_3] - [Cu^{I}(bpy)_2] - [Cu^{II}(bpy)_2] \quad (5)$$

which is a charge-separated species that could undergo charge recombination to return to the initial ground state or alternatively, the electron could self-exchange between neighboring Cu complexes according to:

$$[Ru^{III}(bpy)_2(bpy^{\bullet-})]^* - [Cu^{II}(bpy)_2] - [Cu^{II}(bpy)_2] \rightarrow [Ru^{III}(bpy)_3] - [Cu^{II}(bpy)_2] - [Cu^{I}(bpy)_2] \quad (6)$$

(35) (a) Sutin, N. *Prog. Inorg. Chem.* **1983**, *30*, 441–499. (b) Marcus, R. A.; Siddarth, PIn *Photoprocesses in Transition Metal Complexes, Biosystems and Other Molecules*; Kochanski, E., Ed.; Kluwer Academic Publishers: Netherlands, 1992.

The product in eq 6 would have a greater charge separation distance (and could form by direct electron transfer from the excited state Ru complex), but would also undergo back electron transfer to return to the divalent Ru complex. The time-resolved and temperature dependent data in Table 2 only allow us to conclude that the rate of nonradiative decay is the same for **Ru-4-$(Cu)_2$** and **Ru-5-$(Cu)_2$** and approximately the same as for the **Ru-1-Cu** species, all of which have the same distance between Ru and the closest Cu cross-link. If electron transfer is the quenching mechanism in these systems, differences would expected for the *back* electron transfer rates for **Ru-1-Cu**, **Ru-4-$(Cu)_2$** and **Ru-5-$(Cu)_2$** but these may only be observable in transient absorption experiments that are outside the scope of the current report.

Conclusions

In this paper we have shown the use of flexible artificial oligopeptide construction to prepare a series of $[Ru(bpy)_3]^{2+}$ complexes with pendant bpy ligands that coordinate Cu^{2+} to form $[Cu(bpy)_2]^{2+}$ cross-links. Variation of the oligopeptide sequences provides heterometallic complexes with variable spacing between the Ru and Cu centers and that are di- or trimetallic. The $[Cu(bpy)_2]^{2+}$ cross-links quench the excited state emission of the Ru complex. Time resolved and temperature dependent emission studies point toward an electron transfer quenching mechanism but do not rule out energy transfer. These results demonstrate that self-assembly of structures made from metal coordination based recognition of artificial oligopeptides provide a controlled arrangement of chromophores, electron donors and acceptors in a new approach for mimicking photosynthesis. Absorption and emission maxima, electron transfer rates, and quantum yields are a function of both ligand and metal identity and the distance between them. Interactions between these species are tunable using our modular peptides, providing a readily tailorable set of structures and enabling the construction of more complex architectures and foreshadow a future in which light energy is efficiently harnessed and used. Our ongoing studies aim to use the modular artificial amino acid subunits to construct polyfunctional structures with redox and energy cascades to create long-lived charge-separated states, and to apply time-resolved spectroscopic techniques to study these.

Acknowledgment. We are grateful for financial support from the U.S. Department of Energy (DE-FG02-08ER15986). We thank L. A. Levine for helpful comments for the mass spectrometry experiments.

Supporting Information Available: Synthetic details, supplementary table and figures. This material is available free of charge via the Internet at http://pubs.acs.org.

JA905493X